ACS OMEGA

http://pubs.acs.org/journal/acsodf

Article

Micro-Kelvin Resolution at Room Temperature Using Nanomechanical Thermometry

Elías Ferreiro-Vila, Juan Molina, Lukas M. Weituschat, Eduardo Gil-Santos, Pablo A. Postigo, and Daniel Ramos*

Cite This: *ACS Omega* 2021, 6, 23052–23058

Read Online

ACCESS | Metrics & More | Article Recommendations

ABSTRACT: Ultrahigh sensitivity temperature measurement is becoming increasingly relevant for different scientific and technological fields from fundamental physics to high-precision engineering applications. Here, we demonstrate the use of a nanomechanical resonator—free standing silicon nitride membranes with thicknesses in the nanoscale—for room temperature thermometry reaching an unprecedented resolution of 15 μK. These devices were characterized by using an interferometric system at high vacuum, where there are only two possible mechanisms for heat transfer: thermal conductivity and radiation. While the expected behavior should be to decrease the frequency of the mechanical resonance due to the thermoelastic effect, we observe that the nanomechanical response can be both positive and negative depending on the thermal flux: a heat point source always shifts the mechanical resonance to lower frequencies, while a distributed heat source shifts the resonance to higher frequencies.

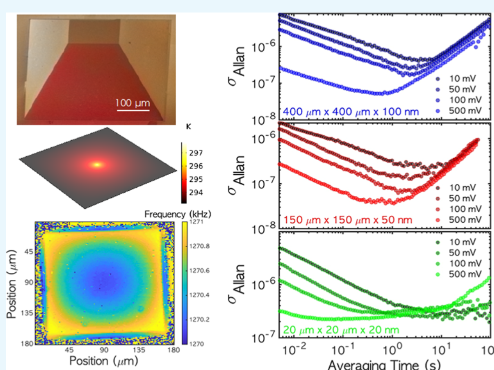

■ INTRODUCTION

Temperature is a crucial variable for many different applications ranging from engineering[1] to fundamental[2] or applied scientific applications.[3,4] Many processes must have either a monitored or a controlled temperature. In order to account for this wide collection of needs, the community has developed a large number of sensors and devices. Until recently, most of the accomplishments for measurement of temperature harness unique properties of materials, traditionally probed using electrical methods.[5,6] However, despite the ubiquity of thermometers, the underlying technology remains unaltered over the last century: both the standard platinum resistance thermometer, developed in the 19th century, and the modern temperature sensors rely on resistance measurements of a thin metal film[7] or a wire. Although resistance thermometers can measure temperature with uncertainties as small as 50 mK, they are sensitive to mechanical shock, thermal stress, and environmental variables such as humidity and chemical contaminants causing drifts and requiring in consequence expensive and time-consuming calibrations.[8,9] Therefore, in recent years, there has been increasing interest in the development of new technologies able to produce new sensing devices to overcome these problems. According to the new definition of the Kelvin adopted in 2018 by the International System of Units, the temperature unit is now based on the exact value of the Boltzmann constant. However, thermodynamic temperature determination (based on the fundamental properties of thermal fluctuations in conductors) remains a complex and heavy task, for example, the resolution at room temperature of a commercially available Johnson noise thermometer is about 100 mK, reaching micro-Kelvin resolution at cryogenic operation temperatures.[10] At low temperature (4 K), the measurement sensitivity can be improved by using a dc-SQUID magnetometer to determine the change in magnetization of a paramagnetic salt,[11] reaching a resolution of about 100 pK, or by using the Coulomb blockade technique to measure the tunnel current in between metallic islands surrounded by an insulator.[12] However, the applicability of these cryogenic techniques is very limited, and they need electrical interactions with the sample through electrical contacts.

The development of temperature sensors using optical or mechanical properties will eventually remove the need for electrical measurements, along with their inherent limitations. Furthermore, the advent of nanomechanics has brought numerous new applications, including temperature sensing[13−16] by using the bimetallic effect. The difference in the

Received: April 16, 2021
Accepted: August 5, 2021
Published: August 27, 2021

© 2021 The Authors. Published by American Chemical Society

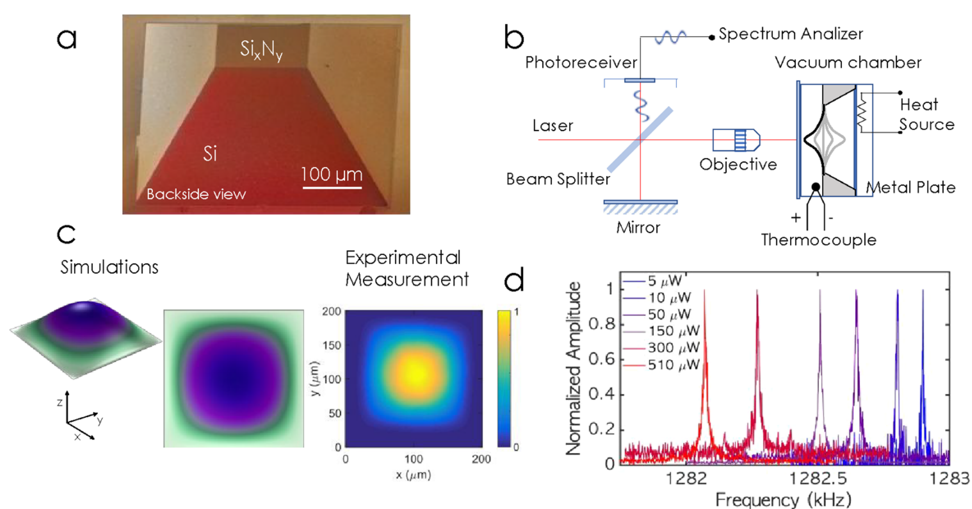

Figure 1. (a) Scanning electron microscopy image of the backside of a 150 μm side silicon nitride membrane. (b) Schematic depiction of the optical readout system. The measurement principle is based on a Michelson interferometer, and the membranes are placed in a high vacuum chamber with a heat source and a thermocouple for calibration purposes. (c) Comparison between the simulated fundamental mechanical mode shape and the experimental measurement (color bar in a.u.). (d) Amplitude spectra of the fundamental mechanical mode for different values of the incident laser power when the laser is focused at the middle point of the membrane.

thermal expansion coefficient of the two layers bends the flexible structure as a consequence of an environmental temperature change.[17] The same principle was successfully used to thermally actuate on these flexible structures by laser absorption[18] or to monitor biological procedures.[19] In order to decrease the noise of the bimetallic effect and consequently increase the measurement resolution, there were increasing efforts in nanomechanical devices made of one material. Because there is no static bending caused by the temperature change in these devices, the measurement principle is based on the study of the dependency of the mechanical resonance frequency as a function of temperature due to thermoelastic effects.[20]

In this work, we have studied the effect of temperature change on nanometer-scale thickness silicon nitride membranes. The thermoelastic effect shifts the mechanical resonance of the membranes to lower frequencies as expected by the theory;[20] however, when the stress comes into play, the resonance shift could be positive or negative depending on the flux direction. The dimensions of the used silicon nitride membranes are 20 μm × 20 μm × 20 nm (f_0 = 8 MHz, $Q \sim 4-5 \times 10^4$), 150 μm × 150 μm × 50 nm (f_0 = 1.28 MHz, $Q \sim 5-6 \times 10^4$), and 400 μm × 400 μm × 100 nm (f_0 = 360 kHz, $Q \sim 4-5 \times 10^3$). The extraordinary low noise of the frequency measurement, with an Allan deviation of about 10^{-8}, allows for a temperature resolution of 15 μK at room temperature for an integration time of about 800 ms, which constitutes an improvement of 4 orders of magnitude with the state-of-the art Johnson noise thermometer and is comparable to optical thermometers based on whispering gallery modes.[21−23]

RESULTS AND DISCUSSION

The membranes were fabricated by using wet back-etch starting from a silicon wafer with a low stress silicon nitride layer on both sides. A square is opened on the wafer back side by photolithography, subsequently followed by dry etch. The exposed silicon was subsequently wet-etched from the back side until it was stopped by the low stress silicon nitride of the front side, revealing the crystallographic planes of the silicon, as shown in Figure 1a. The mechanical modes of the released membranes were optically measured by using a homemade Michelson interferometer, as shown in Figure 1b. A collimated laser beam (Toptica Photonics AG, TopMode 633 nm) is split up into two beams by means of a beam splitter: one directed to a reference mirror and one focused on the membrane, which is placed in a high vacuum chamber (final working pressure 10^{-7} mbar) by means of a long working distance microscope objective (Mitutoyo 20 × 0.42 NA). The reflected laser beams are recombined and collected by a photoreceiver. The signal coming out from the photoreceiver is amplified and analyzed by a spectrum analyzer. The samples are mounted on a 3D position stage (Attocube systems AG) allowing to sweep the laser across the sample with a precision of 50 nm. The amplitude maps, obtained by measuring the mechanical amplitude spectra at different points along the membrane, are used to visualize the mechanical mode shape, as shown in Figure 1c, showing a very good agreement with the expected mechanical mode profile simulated by finite element method (FEM, Comsol Multiphysics) by using the following values for the Young's modulus: E = 250 GPa, mass density, ρ = 3100 kg·m^{-3}, and Poisson's ratio, ν = 0.23. Thanks to the closed loop functionality of the position system, it is possible to focus the laser spot always on the same point during the whole experiment with a position repeatability of 50 nm, for example, at the membrane center point while changing the laser power, as shown in Figure 1d. The measured spectra clearly show a dependency of the mechanical resonance frequency of the silicon nitride membrane with the laser power. The lower the power, the higher the mechanical resonance frequency. In Figure 1d, we show 6 different spectra obtained at 510, 300, 150, 50, 10, and 5 μW, with the corresponding frequencies ranging from 1282.1 up to 1282.9 kHz.

In order to gain insights about the physical process behind the frequency shift as a function of laser power, we have performed finite element simulations (Comsol Multiphysics). There are two opposite effects when illuminating a free-standing mechanical structure with a laser: radiation pressure and bolometric effects.[4,24] Radiation pressure is the result of

https://doi.org/10.1021/acsomega.1c02045
ACS Omega 2021, 6, 23052−23058

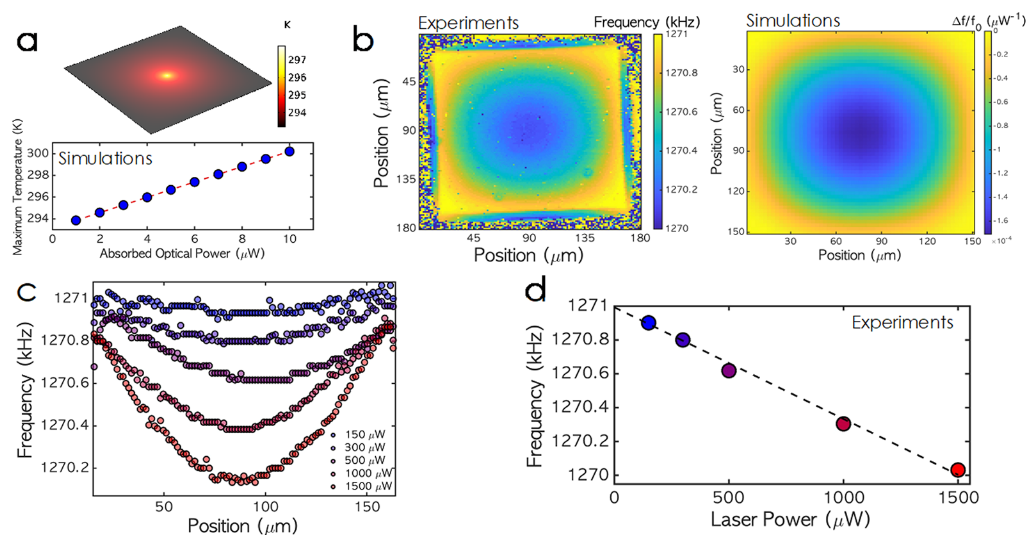

Figure 2. Hot spot experiments. (a) Finite element simulation of the temperature profile when a laser is focused at the center point of a suspended silicon nitride membrane. (b) Left. Experimental mechanical resonance frequency measured at different points forming a 2D matrix over the suspended membrane. The minimal frequency is measured when the laser is focused at the membrane center. Right. Finite element simulations of the relative frequency shift per unit of absorbed power for the fundamental mechanical mode of the silicon nitride membrane by sweeping a gaussian heat source with a size of 2 μm over the surface. (c) Experimental resonance frequency as a function of the position along the middle axis of the membrane for different laser powers. (d) Experimental resonance frequency shift as a function of the laser power when focused at the middle point of the membrane; the dashed line is a linear fit of the results.

the inelastic momentum transfer between the photons and the mechanical structure. It depends on the laser power, wavelength, and material refractive index. The most general way to calculate the radiation pressure force is by integrating Maxwell's stress tensor over a closed path surrounding the flexible structure,[25] $F_\alpha = \sum_\beta \oint T_{\alpha\beta} n_\beta \mathrm{d}l$, where the Maxwell stress tensor is given by $T_{\alpha\beta} = \varepsilon E_\alpha E_\beta^* + \mu H_\alpha H_\beta^* - \frac{1}{2}\delta_{\alpha\beta}(\varepsilon |E|^2 + \mu |H|^2)$, where $\hat{n}$ is a unit vector normal to the integration path pointing outward, μ is the permeability, and $\vec{E}$ and $\vec{H}$ are the electric and magnetic fields, respectively, which are those obtained by solving Maxwell's equations. The calculations show that the radiation pressure is negligible for the used laser powers. Therefore, the mechanical frequency shift must be caused by thermal effects. The thermal profile over the membrane is calculated by solving the following equation

$$\rho C_\mathrm{p}\left(\frac{\partial T}{\partial t} + \vec{u}_\mathrm{trans}\cdot\nabla T\right) + \nabla\cdot(\vec{q} + \vec{q}_\mathrm{r}) = -\alpha T\frac{\mathrm{d}S}{\mathrm{d}t} + Q \quad (1)$$

where ρ is the density, C_p is the specific heat capacity at constant stress, T is the absolute temperature, $\vec{u}_\mathrm{trans}$ is the velocity vector of translational motion, $\vec{q}$ is the heat flux by conduction, $\vec{q}_\mathrm{r}$ is the heat flux by radiation, α is the coefficient of thermal expansion, S is the second Piola−Kirchhoff stress tensor, and Q contains all the additional heat sources. Please note that the right-hand term accounts for thermoelastic effects in solids. For the silicon nitride membrane, $\alpha_\mathrm{SiN} = 2.3 \times 10^{-6}$ K^{-1}, $C_\mathrm{pSiN} = 700$ J · kg^{-1} · K^{-1}, and for the silicon frame, $\alpha_\mathrm{Si} = 2.6 \times 10^{-6}$ K^{-1}, $C_\mathrm{pSi} = 710$ J · kg^{-1} · K^{-1}.

We have simulated a gaussian laser beam focused on the silicon nitride surface, as shown in Figure 2a. The absorbed power is translated into a heat source, and the temperature distribution of the whole structure is calculated.[26,27] In order to mimic the experimental conditions, the membrane boundaries are considered as a heat sink at room temperature. Because the experiments were carried out at high vacuum, in the simulations, we take into account only two thermal transport mechanisms: the heat loss by radiation and the thermal conductivity through the structure. Therefore, the temperature is maximal at the illumination region and exponentially decays until reaching room temperature at the membrane borders. The temperature of the illuminated region depends linearly on the laser power, as can be seen from the lower chart in Figure 2a. As it was anticipated by the power-dependent measurements, the mechanical resonance frequency of the membrane depends on the temperature. Therefore, the measured resonant frequency depends on the coordinates of the focused laser spot on the membrane, as shown in Figure 2b. According to previous works in literature,[28] given the isotropy in the thermal transport properties of silicon nitride, by sweeping a laser spot at fixed power (1500 μW), we experimentally observe a radial dependence of the resonance frequency, being the minimal at the membrane center ($\Delta f = -0.7$ kHz), as shown by the right colormap in Figure 2b. It is possible to simulate these experimental results by combining three different physical models in FEM software (Comsol Multiphysics): electromagnetic waves to calculate the absorbed power by the material, thermal transport to calculate the temperature distribution at the membrane, and structural dynamics to calculate the resonance frequency of the membrane when shining at a single point. By sweeping this shining point all along the membrane, we can reconstruct the experimental results, as shown in the left colormap in Figure 2b. These experiments are performed at different laser powers ranging from 150 up to 1500 μW, as shown in Figure 2c. For comparison in between the different laser powers, we plot the resonance frequencies by sweeping over the same line across the membrane while increasing the power. The frequency shift when the laser spot is focused at the membrane center depends linearly on the laser power,[28] as shown in Figure 2d.

In order to perform the temperature calibration, we have introduced a heat source inside the vacuum chamber and a

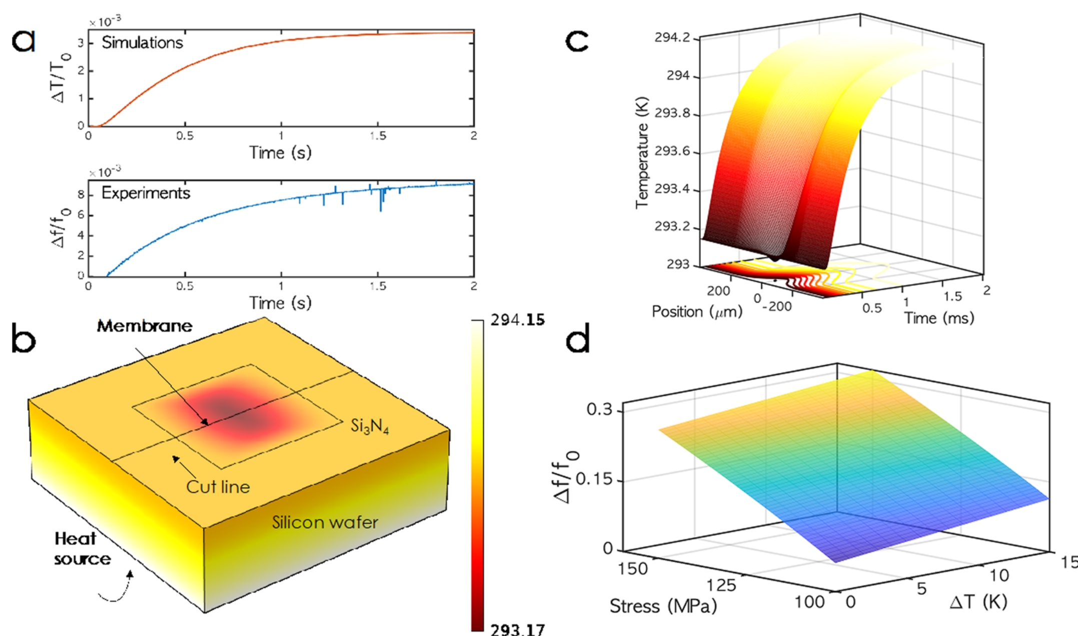

Figure 3. Distributed heat source. (a) Time response of the system to a temperature increment. Upper chart. Simulated relative temperature rise as a function of time. Lower chart. Experimental relative frequency shift as a function of time. (b) FEM simulation of the temperature profile of the whole structure by heating the lower side of the silicon frame. In order to mimic the experimental high vacuum conditions, there is only heat flux by conduction and radiation by the material surfaces. (c) Simulated time evolution of the temperature profile along the cut line drawn in b. (d) FEM simulation of the relative resonance frequency shift of the mechanical frequency mode as a function of initial stress and temperature change.

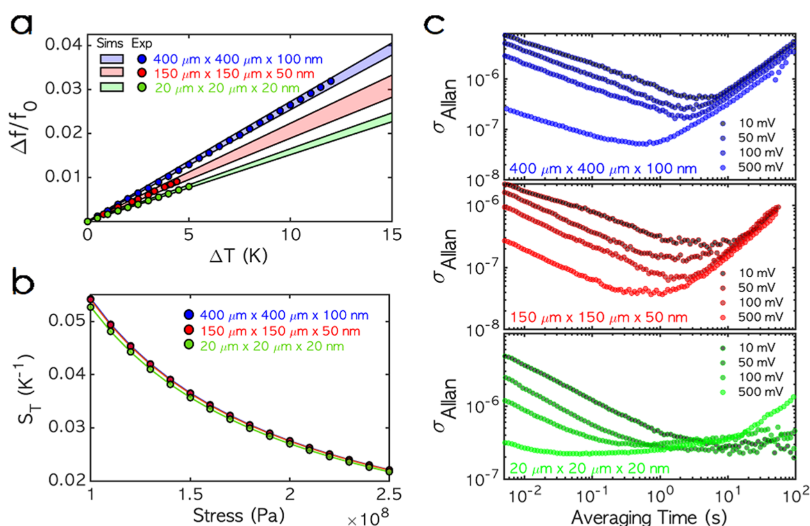

Figure 4. Nanomechanical thermometry performance. (a) Relative frequency shift as a function of temperature variation for three different silicon nitride membrane geometries: squares of 400 μm lateral size and 100 nm in thickness (blue symbols), 150 μm length square membranes of 50 nm in thickness (red symbols), and 20 μm length square membranes of 20 nm in thickness (green symbols). The shadowed areas correspond to the FEM simulations of the response. (b) Multiphysics FEM simulation of the thermal sensitivity as a function initial stress for the 400 μm membranes (blue symbols and line, hidden by the red symbols), the 150 μm membranes (red symbols and line), and 20 μm membranes (green symbols and line). (c) Experimental Allan deviation for the different membrane geometries (upper chart for the 400 μm membranes, middle chart for the 150 μm membranes, and lower chart for the 20 μm membranes) for different piezo excitation ranging from 10 up to 500 mV.

thermocouple, as it was previously described in Figure 1b. The heat source is placed in thermal contact with the silicon frame; therefore, the silicon is now hotter than the membrane. When the system temperature rises, we observe the opposite effect on the mechanical properties of the membrane compared with the laser local heating; the mechanical resonance is shifted to higher frequencies as temperature increases. The thermal process is very slow, with a time constant of the order of seconds, as shown in Figure 3a. With the aim of shedding light on this effect, we have to perform time-dependent simulations of the heat flux in the whole structure, as shown in Figure 3b. Now, the heat source is the bottom side of the silicon wafer. Because the chip is located inside a high vacuum chamber, the heat flux is only due to conduction and radiation. Therefore, at the stationary state, the silicon chip frame is hotter than the suspended silicon nitride membrane. The difference in the thermal expansion coefficient of the membrane and the frame

https://doi.org/10.1021/acsomega.1c02045
ACS Omega 2021, 6, 23052−23058

introduces a tensile stress in the membrane shifting the resonance to higher values.

In order to reach the stationary state, the heat must be conductively transported from the bottom wafer side.[29] In Figure 3c, we show the time evolution of the simulated temperature profile along the cut line, which is shown in Figure 3b. The time the heat needs to flow from the bottom wafer side to reach the membrane depends on the material thermal transport properties. Considering that the heat flux is only determined by conductivity and heat loss by radiation, the time to reach the stationary temperature is significant. By solving eq 1, we can obtain the time dependency of the temperature difference and therefore the frequency dependency with time, as shown in Figure 3a in the upper chart. The frequency sensitivity[30−32] can be calculated as

$$S_f(T) = \frac{1}{f(T_0)} \frac{\partial f(T)}{\partial T}\bigg|_{T=T_0} = -\frac{\alpha E}{2\sigma} \tag{2}$$

where E is the Young's modulus, σ is the initial stress, and f is the resonance frequency of the membrane, which can be calculated as

$$f = \frac{\sqrt{2}}{2L}\sqrt{\frac{\sigma}{\rho}} \tag{3}$$

where L is the length of the square, and ρ is the mass density of the structural material of the membrane, silicon nitride in this case.

From eq 2, the mechanical frequency sensitivity to a temperature change is inversely proportional to the initial stress of the structural material. The larger the stress, the lower is the sensitivity. Figure 3d shows the simulated normalized frequency response of a square silicon nitride membrane of 150 μm lateral size and 50 nm thickness. We have simulated the stationary frequency resonance for the fundamental mechanical mode, while changing the initial stress for different temperatures increases by using FEM calculation, generating a 3D surface. While the frequency increases with the initial stress, according to eq 3, its variation with temperature (the slope representing the sensitivity) decreases, which agrees with our theoretical modeling (eq 2).

As it has been noted before, stress plays a critical role; the sensitivity of the nanomechanical thermometry is inversely proportional to the membrane initial stress. Based on the geometry measured by scanning electron microscopy, and the mechanical resonance frequency of the fundamental mode, it is possible to calculate the stress of each membrane (140 ± 5 MPa for the 400 μm membrane, 200 ± 5 MPa for the 150 μm membrane, and 230 ± 10 MPa for the 20 μm membrane). Note that the smaller the membrane, the higher is the structural stress. This is due to the fabrication process and the stress release by suspended structures.[27] In Figure 4a, we show the relative frequency shift for different membranes as a function of temperature for an incident laser power of 50 μW. The slope of this measurement gives us the responsivity of the system, $\mathcal{R} = {}^{(\Delta f/f_0)}/_{\Delta T}$. The largest responsivity is shown by the larger membrane (0.0025 K^{-1} for the 400 μm membrane, blue symbols in Figure 4a) and the smallest responsivity by the 20 μm membrane, 0.0015 K^{-1} (green symbols in Figure 4a), the 150 μm membrane being an intermediate response, 0.002 K^{-1} (red symbols in Figure 4a). The shadowed areas correspond to the FEM simulated response, the variability being due to the abovementioned variability in the structural stress. As can be seen from Figure 4a, the agreement between the simulations and the experiments is excellent. The stress dependency of the sensitivity (eq 2) has been simulated by FEM, as shown in Figure 4b, which is very similar for all simulated membranes. Actually, the observed small differences correspond to second-order variations in geometry. Note that from the 20 to the 400 μm membrane, the thickness increases by a factor of 5. Finally, the performance of the thermal sensor is characterized by the minimum measurable frequency variation, that is, the frequency noise of the system. The way to calculate the noise level of the readout system is through the Allan deviation calculation, $\sigma_{\text{Allan}}(\tau) = \sqrt{{\sigma_{\text{Allan}}}^2(\tau)}$, where ${\sigma_{\text{Allan}}}^2(\tau)$ is defined as the Allan variance, which is calculated from the average of the frequencies measured in a temporal integration time τ, ${\sigma_{\text{Allan}}}^2(\tau) = {}^1/_2(\bar{f}(t+\tau) - \bar{f}(t))^2$. According to previous works in literature,[33,34] the frequency stability improves as the driving voltage of a piezo shaker placed close to the sample is increased, which leads to a decrease in the Allan deviation, as shown in Figure 4c. The Allan deviation reaches a value of 4×10^{-8} for the 400 μm membrane, 3×10^{-8} for the 150 μm membrane, and $1{\times}10^{-7}$ for the 20 μm membrane for integration times of about 800 ms in all the cases. For the 150 μm membrane, given the fundamental resonance frequency of 1.2 MHz, this Allan variance means that we have a frequency instability of δf = 36 mHz RMS. By taking into account the value of the responsivity, the temperature resolution is given by $\delta T = \frac{\delta f}{f_0 \mathcal{R}}$, reaching a minimal value of 1.5×10^{-5} K = 15 μK for the 150 μm membrane.

CONCLUSIONS

In conclusion, we have experimentally demonstrated the use of a nanomechanical resonator for ultrahigh thermometry resolution at room temperature, with a value of about 15 μK. The working principle is based on the low-noise measurement of the effect of the temperature rise on the mechanical resonance frequency of suspended low-stress silicon nitride membranes. These membranes were experimentally characterized by using a Michelson interferometer in high vacuum, where there are only two possible mechanisms for heat transfer: thermal conductivity and radiation. While the expected behavior should be to decrease the mechanical resonance frequency due to the thermoelastic effect, we realized that the nanomechanical response of the membrane to a temperature rise can be both positive and negative depending on the temperature distribution and the generated stress in the structure. A heat point source located on the membrane always shifts the fundamental mechanical resonance to lower frequencies, while a distributed heat source over the silicon wafer, which serves as a supporting frame for the silicon nitride membrane, shifts the resonance to higher frequencies.

AUTHOR INFORMATION

Corresponding Author

Daniel Ramos − *Instituto de Micro y Nanotecnología, IMN-CNM (CSIC), E-28760 Tres Cantos, Madrid, Spain;* orcid.org/0000-0003-2677-4058; Email: daniel.ramos@csic.es

https://doi.org/10.1021/acsomega.1c02045
ACS Omega 2021, 6, 23052−23058

Authors

Elías Ferreiro-Vila − *Instituto de Micro y Nanotecnología, IMN-CNM (CSIC), E-28760 Tres Cantos, Madrid, Spain*
Juan Molina − *Instituto de Micro y Nanotecnología, IMN-CNM (CSIC), E-28760 Tres Cantos, Madrid, Spain*
Lukas M. Weituschat − *Instituto de Micro y Nanotecnología, IMN-CNM (CSIC), E-28760 Tres Cantos, Madrid, Spain*
Eduardo Gil-Santos − *Instituto de Micro y Nanotecnología, IMN-CNM (CSIC), E-28760 Tres Cantos, Madrid, Spain*
Pablo A. Postigo − *Instituto de Micro y Nanotecnología, IMN-CNM (CSIC), E-28760 Tres Cantos, Madrid, Spain*

Complete contact information is available at:
https://pubs.acs.org/10.1021/acsomega.1c02045

Author Contributions

D.R. and P.A.P. conceived and designed the work. E.F.-V. and J. M. characterized the devices and performed the thermometry experiments. E. F.-V. and E.G.-S. performed the Allan variance measurements. L.M.W. and D.R. performed the simulations. D.R. wrote the manuscript with input from all authors. All authors analyzed the data, discussed the results, and commented on the manuscript.

Notes

The authors declare no competing financial interest.

■ ACKNOWLEDGMENTS

This research is funded by the Spanish Ministry of Science under project MOMPs reference TEC2017-89765-R and the European Association of National Metrology Institutes (JRP f14 PhotOQuanT—17FUN05). E.G.-S acknowledges financial support by the Spanish Ministry of Science under the project MicroBIOMS, reference PID2019-109765RA-I00. This project has received funding from the EMPIR program co-financed by the Participating States and from the European Union's Horizon 2020 research and innovation program. The service from the Micro and Nanofabrication Laboratory (MiNa) and X-SEM Laboratory is funded by MCIU (CSIC13-4E-1794) and EU (FEDER, FSE).

■ REFERENCES

(1) Saito, S.; Tanaka, T.; Sudo, Y. *Design of high temperature Engineering Test Reactor (HTTR)*. Japan Atomic Energy Research Inst.: Tokyo, Japan, 1994, p. 268.
(2) Genet, C.; Lambrecht, A.; Reynaud, S. Temperature dependence of the Casimir effect between metallic mirrors. *Phys. Rev. A* **2000**, *62*, No. 012110.
(3) Somero, G. N. Proteins and Temperature. *Annu. Rev. Physiol.* **1995**, *57*, 43−68.
(4) Gil-Santos, E.; Ramos, D.; Pini, V.; Llorens, J.; Fernández-Regúlez, M.; Calleja, M.; Tamayo, J.; San Paulo, A. Optical back-action in silicon nanowire resonators: bolometric versus radiation pressure effects. *New J. Phys.* **2013**, *15*, No. 035001.
(5) Majumdar, A.; Lai, J.; Chandrachood, M.; Nakabeppu, O.; Wu, Y.; Shi, Z. Thermal imaging by atomic force microscopy using thermocouple cantilever probes. *Rev. Sci. Instrum.* **1995**, *66*, 3584−3592.
(6) Marie, R.; Thaysen, J.; Christensen, C. B. V.; Boisen, A. A cantilever-based sensor for thermal cycling in buffer solution. *Microelectron. Eng.* **2003**, *67-68*, 893−898.
(7) Boisen, A.; Thaysen, J.; Jensenius, H.; Hansen, O. Environmental sensors based on micromachined cantilevers with integrated read-out. *Ultramicroscopy* **2000**, *82*, 11−16.
(8) King, W. P.; Bhatia, B.; Felts, J. R.; Kim, H. J.; Kwon, B.; Lee, B.; Somnath, S.; Rosenberger, M. Heated Atomic Force Microscope Cantilevers and their Applications. *Annu. Rev. Heat Transfer* **2013**, *16*, 287−326.
(9) Sadat, S.; Meyhofer, E.; Reddy, P. High resolution resistive thermometry for micro/nanoscale measurements. *Rev. Sci. Instrum.* **2012**, *83*, No. 084902.
(10) Qu, J. F.; Benz, S. P.; Rogalla, H.; Tew, W. L.; White, D. R.; Zhou, K. L. Johnson noise thermometry. *Meas. Sci. Technol.* **2019**, *30*, 112001.
(11) Fu, H.; Baddar, H.; Kuehn, K.; Larson, M.; Mulders, N.; Schegolev, A.; Ahlers, G. A High-Resolution Thermometer for the Range 1.6 to 5 K. *J. Low Temp. Phys.* **1998**, *111*, 49−71.
(12) Purdy, T. P.; Singh, R.; Klimov, N. N.; Ahmed, Z.; Grutter, K.; Srinivasan, K.; Taylor, J. M. Optomechanical Quantum Thermometry. In *Conference on Lasers and Electro-Optics*, 2018.
(13) Toda, M.; Inomata, N.; Ono, T.; Voiculescu, I. Cantilever beam temperature sensors for biological applications. *IEEJ Trans. Electr. Electron. Eng.* **2017**, *12*, 153−160.
(14) Mertens, J.; Finot, E.; Thundat, T.; Fabre, A.; Nadal, M.-H.; Eyraud, V.; Bourillot, E. Effects of temperature and pressure on microcantilever resonance response. *Ultramicroscopy* **2003**, *97*, 119−126.
(15) Thundat, T.; Warmack, R. J.; Chen, G. Y.; Allison, D. P. Thermal and ambient-induced deflections of scanning force microscope cantilevers. *Appl. Phys. Lett.* **1994**, *64*, 2894−2896.
(16) Heidarpour Roshan, M.; Zaliasl, S.; Joo, K.; Souri, K.; Palwai, R.; Chen, L. W.; Singh, A.; Pamarti, S.; Miller, N. J.; Doll, J. C.; Arft, C.; Tabatabaei, S.; Sechen, C.; Partridge, A.; Menon, V. A MEMS-Assisted Temperature Sensor With 20- μK Resolution, Conversion Rate of 200 S/s, and FOM of 0.04 pJK2. *IEEE J. Solid-State Circuits* **2017**, *52*, 185−197.
(17) Ramos, D.; Tamayo, J.; Mertens, J.; Calleja, M. Photothermal excitation of microcantilevers in liquids. *J. Appl. Phys.* **2006**, *99*, 124904.
(18) Ramos, D.; Mertens, J.; Calleja, M.; Tamayo, J. Phototermal self-excitation of nanomechanical resonators in liquids. *Appl. Phys. Lett.* **2008**, *92*, 173108.
(19) Domínguez, C. M.; Ramos, D.; Mendieta-Moreno, J. I.; Fierro, J. L. G.; Mendieta, J.; Tamayo, J.; Calleja, M. Effect of water-DNA interactions on elastic properties of DNA self-assembled monolayers. *Sci. Rep.* **2017**, *7*, 536.
(20) Ramos, D.; Malvar, O.; Davis, Z. J.; Tamayo, J.; Calleja, M. Nanomechanical Plasmon Spectroscopy of Single Gold Nanoparticles. *Nano Lett.* **2018**, *18*, 7165.
(21) Strekalov, D. V.; Thompson, R. J.; Baumgartel, L. M.; Grudinin, I. S.; Yu, N. Temperature measurement and stabilization in a birefringent whispering gallery mode resonator. *Opt. Express* **2011**, *19*, 14495−14501.
(22) Weng, W.; Anstie, J. D.; Stace, T. M.; Campbell, G.; Baynes, F. N.; Luiten, A. N. Nano-Kelvin Thermometry and Temperature Control: Beyond the Thermal Noise Limit. *Phys. Rev. Lett.* **2014**, *112*, No. 160801.
(23) Weng, W.; Light, P. S.; Luiten, A. N. Ultra-sensitive lithium niobate thermometer based on a dual-resonant whispering-gallery-mode cavity. *Opt. Lett.* **2018**, *43*, 1415−1418.
(24) Ramos, D.; Gil-Santos, E.; Pini, V.; Llorens, J. M.; Fernández-Regúlez, M.; San Paulo, A.; Calleja, M.; Tamayo, J. Optomechanics with Silicon Nanowires by Harnessing Confined Electromagnetic Modes. *Nano Lett.* **2012**, *12*, 932−937.
(25) Hui, P.-C.; Woolf, D.; Iwase, E.; Sohn, Y.-I.; Ramos, D.; Khan, M.; Rodriguez, A. W.; Johnson, S. G.; Capasso, F.; Loncar, M. Optical bistability with a repulsive optical force in coupled silicon photonic crystal membranes. *Appl. Phys. Lett.* **2013**, *103*, No. 021102.
(26) Kiracofe, D.; Kobayashi, K.; Labuda, A.; Raman, A.; Yamada, H. High efficiency laser photothermal excitation of microcantilever vibrations in air and liquids. *Rev. Sci. Instrum.* **2011**, *82*, No. 013702.
(27) Pini, V.; Tamayo, J.; Gil-Santos, E.; Ramos, D.; Kosaka, P.; Tong, H.-D.; van Rijn, C.; Calleja, M. Shedding Light on Axial Stress Effect on Resonance Frequencies of Nanocantilevers. *ACS Nano* **2011**, *5*, 4269−4275.

(28) Islam, A.; van den Akker, A.; Feng, P. X. L. Anisotropic Thermal Conductivity of Suspended Black Phosphorus Probed by Opto-Thermomechanical Resonance Spectromicroscopy. *Nano Lett.* **2018**, *18*, 7683−7691.
(29) Landry, E. S.; McGaughey, A. J. H. Effect of film thickness on the thermal resistance of confined semiconductor thin films. *J. Appl. Phys.* **2010**, *107*, No. 013521.
(30) Childs, P. R. N.; Greenwood, J. R.; Long, C. A. Review of temperature measurement. *Rev. Sci. Instrum.* **2000**, *71*, 2959−2978.
(31) Larsen, T.; Schmid, S.; Grönberg, L.; Niskanen, A. O.; Hassel, J.; Dohn, S.; Boisen, A. Ultrasensitive string-based temperature sensors. *Appl. Phys. Lett.* **2011**, *98*, 121901.
(32) Piller, M.; Sadeghi, P.; West, R. G.; Luhmann, N.; Martini, P.; Hansen, O.; Schmid, S. Thermal radiation dominated heat transfer in nanomechanical silicon nitride drum resonators. *Appl. Phys. Lett.* **2020**, *117*, No. 034101.
(33) Sansa, M.; Sage, E.; Bullard, E. C.; Gély, M.; Alava, T.; Colinet, E.; Naik, A. K.; Villanueva, L. G.; Duraffourg, L.; Roukes, M. L.; Jourdan, G.; Hentz, S. Frequency fluctuations in silicon nanoresonators. *Nat. Nanotechnol.* **2016**, *11*, 552−558.
(34) Ekinci, K. L.; Yang, Y. T.; Roukes, M. L. Ultimate limits to inertial mass sensing based upon nanoelectromechanical systems. *J. Appl. Phys.* **2004**, *95*, 2682−2689.

https://doi.org/10.1021/acsomega.1c02045
ACS Omega 2021, 6, 23052−23058